Real-Time Measurements of Local Myocardium Motion and Arterial Wall Thickening

Hiroshi Kanai, *Member, IEEE*, Yoshiro Koiwa, and Jianping Zhang

***Abstract*—We have already developed a new method, namely, the phased tracking method, to track the movement of the heart wall and arterial wall accurately based on both the phase and magnitude of the demodulated signals to determine the instantaneous position of an object. This method has been realized by an off-line measurement system, which cannot be applied to transient evaluation of rapid response of the cardiovascular system to physiological stress. In this paper, therefore, a real-time system to measure change in the thickness of the myocardium and the arterial wall is presented. In this system, an analytic signal from standard ultrasonic diagnostic equipment is analogue-to-digital (A/D) converted at a sampling frequency of 1 MHz. By pipelining and parallel processing using four high-speed digital signal processing (DSP) chips, the method just described is realized in real time. The tracking results for both sides of the heart and/or arterial wall are superimposed on the M (motion)-mode image in the work station (WS), and the thickness changes of the heart and/or arterial wall are also displayed and digital-to-analogue (D/A) converted in real time. From the regional change in thickness of the heart wall, spatial distribution of myocardial motility and contractility can be evaluated. For the arterial wall, its local elasticity can be evaluated by referring to the blood pressure. In in vivo experiments, the rapid response of the change in wall thickness of the carotid artery to the dose of the nitroglycerine (NTG) is evaluated. This new real-time system offers potential for quantitative diagnosis of myocardial motility, early stage atherosclerosis, and the transient evaluation of the rapid response of the cardiovascular system to physiological stress.**

I. Introduction

In the interventricular septum (IVS) and the posterior wall of the left ventricle (LV) shown in Fig. 1(1-a), thickening and thinning periodically occur during myocardial contraction and relaxation as illustrated in Fig. 1(1-b) and (1-c). This thickening and thinning in each local area of the heart wall corresponds to the regional myocardial motility, which originates from the sliding of the myosin and actin fibers. To realize this evaluation transcutaneously using ultrasound, it is necessary to track the instantaneous positions $x_A(t)$ and $x_B(t)$ of the two points, A and B, which are preset at the end-diastole along the ultrasonic beam in the IVS or the posterior wall. Then, the change in thickness, $\Delta h_{AB}(t)$, between these two points A and B from their thickness $h_{AB}(t_0)$ at the end-diastole is obtained from the difference between $x_A(t)$ and $x_B(t)$ as illustrated in Fig. 1(1-c) if the ultrasonic beam is almost perpendicular to the wall during the cardiac cycle [1].

In the heart, there are complex movements, that is, torsional, sagittal, and horizontal movements, especially during cardiac contraction. However, as shown by the magnetic resonance (MR) tagging pattern, there are far fewer torsional, sagittal, and horizontal movements in the IVS compared with those in the right ventricular anterior wall, the LV posterior wall, and the apex [2]. Thus, our measurements have been applied to the IVS to eliminate complexity of the three-dimensional motions during the cardiac cycle [1],[3].

As for the arterial wall, in the ejection period, the pressure wave comes from the LV and expands the lumen. Thus, the arterial wall becomes slightly thin during the ejection period. In the literature, measurement of the change in diameter, $\Delta d_{BA'}(t)$, of the lumen has been reported. From $\Delta d_{BA'}(t)$, the elasticity of the arterial wall can be diagnosed by assuming that it is homogeneously changed in the circumferential direction because of atherosclerosis.

On the other hand, measurement of the change in thickness makes it possible to evaluate the elasticity of the arterial wall in each local area; the locality in the circumferential direction is indispensable to diagnosis of the inner characteristics of atherosclerotic plaque. For this purpose, by tracking the instantaneous positions, $x_A(t)$ and $x_B(t)$, which are, respectively, preset to $x_A(t_0)$ and $x_B(t_0)$ at the end diastole along the ultrasonic beam in the arterial wall as illustrated in Fig. 1(2-b), the small change in wall thickness, $\Delta h_{AB}(t)$, between these two points, A and B, is obtained as illustrated in Fig. 1(2-c) if the ultrasonic beam is almost perpendicular to the wall. From the ratio of the change in thickness, $\Delta h_{AB}(t)$, to the thickness, $h_{AB}(t_0)$, between these points preset at the end diastole, the deformation is obtained. If the deformation is sufficiently small and is in the linear regime, it shows the strain and the regional elasticity of the wall can be approximately evaluated using the pulse pressure measured at the brachial artery [4]. Therefore, the transcutaneous measurement of the change in thickness of the regional area of the heart wall or the arterial wall during each cardiac cycle provides the essential tools for diagnosis of heart diseases or atherosclerosis.

Manuscript received September 29, 1998; accepted March 25, 1999. This work was supported in part by a Grant-in-Aid for Scientific Research from the Ministry of Education, Science and Culture of Japan.

H. Kanai is with the Department of Electrical Engineering, Graduate School of Engineering, Tohoku University, Sendai 980-8579, Japan (e-mail: hkanai@ecei.tohoku.ac.jp).

Y. Koiwa is with the First Department of Internal Medicine, Tohoku University School of Medicine, Seiryou-machi, Aoba-ku, Sendai 980-8574, Japan.

J. Zhang is with Section 2, Technical Division, Systems Design Service Corporation, Daito Building 3F, Takada 3-32-1, Toshiama-ku, Tokyo 171, Japan.

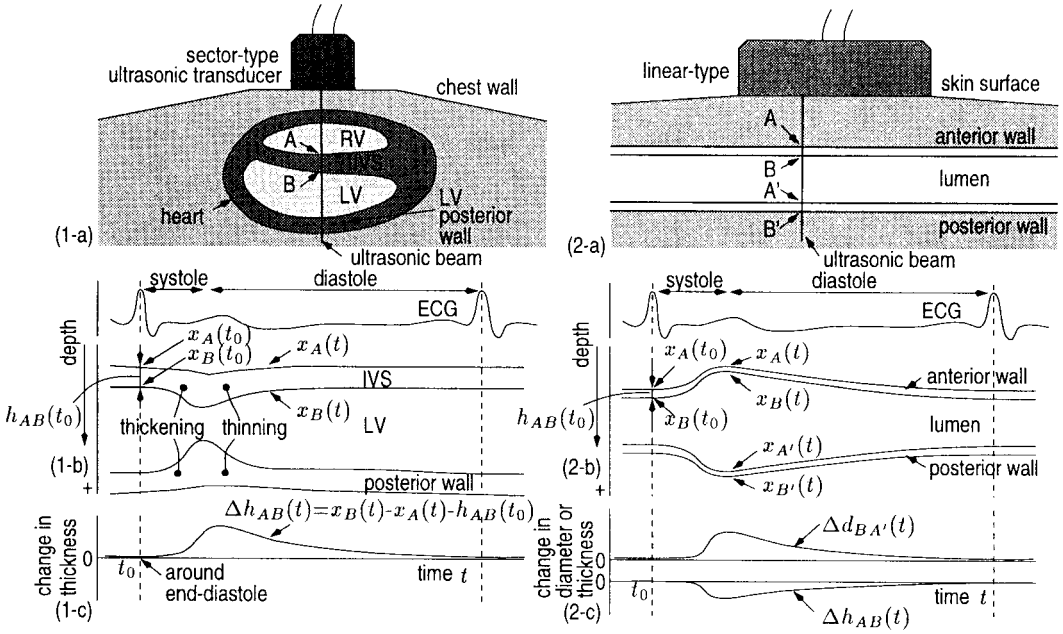

Fig. 1. An illustration explaining the procedure of measuring the change in thickness, $\Delta h_{AB}(t)$, of the heart/arterial wall, and the change in diameter, $\Delta d_{BA'}(t)$, of the lumen by tracking the movement $x_A(t)$ and $x_B(t)$ of points A and B respectively, preset in the heart wall and arterial wall along the ultrasonic beam. (1) for the IVS; (2) for the arterial wall. (a) Cross-sectional image, (b) displacement $x_A(t)$ and $x_B(t)$, (c) change in thickness, $\Delta h_{AB}(t)$, of the heart/arterial wall and change in diameter, $\Delta d_{BA'}(t)$.

The accuracy required for the simultaneous measurement of the instantaneous positions $x_A(t)$ and $x_B(t)$ of points A and B is estimated as follows. For the IVS, for example, the thickness is about 10 mm for a normal young adult, and the change in thickness is approximately 1 to 3 mm during one cardiac cycle [3]. Thus, when the distance of 0.75 mm between these two points in the LV wall is preset at the end diastole, the minimum value of the thickness change, $\Delta h_{AB}(t)$, between these points is approximately 75 μm. For the carotid artery, on the other hand, the thickness of the wall is about 1 mm, and the change in thickness, $\Delta h_{AB}(t)$, is less than 100 μm during one cardiac cycle in normal adults [4].

For either case, therefore, the necessary spatial resolution in the measurement of instantaneous position as a waveform is at least 10 μm. If the velocity signals $v_A(t)$ and $v_B(t)$ of these two points, A and B, are detected based on the pulse Doppler method, the necessary accuracy of the velocity measurement is about 10 μm/200 μs =0.05 m/s when the pulse repetition frequency (PRF) of the transmission-pulse train is 5 kHz (=1/200 μs). If the equivalent sampling period of the velocity signal $v_i(t)$ is longer than 200 μs as in the FFT (fast Fourier transform)-based standard Doppler system, for example, more accurate velocity measurement is required. Because there is motion with large amplitude (about $\pm$10 mm) caused by the heartbeat at the point in the LV wall, moreover, the dynamic range required for the measurement of the movement is about 1000 (10 mm/10 μm) = 60 dB in amplitude.

Though M-mode echocardiography offers an advantage in critically examining at the motion pattern of the LV, its spatial resolution along the ultrasonic beam is limited to a few wavelengths, namely, at most about 1 mm for ultrasound of 3 MHz because an M-mode image is displayed based on the amplitude of the reflected ultrasound. On the other hand, there have been numerous elaborate techniques proposed for noninvasive measurement of the velocity of the blood flow in the heart or the arteries based on the Doppler effect [5]–[14]. Moreover, several methods, including the phase-locked-loop (PLL) techniques, have been proposed to measure rough changes in the diameter of the arterial walls by tracking arterial wall displacement in real time [15]–[33].

For the accurate detection of the velocity signal, that is, the instantaneous movement, on or in the heart wall or arterial wall, we have developed the following phased tracking method [3]. Using this method, by calculating the auto-correlation function under the constraint least mean square technique between the sequentially received echoes, the phase change caused by movement of the preset point (i) during the pulse repetition period ΔT(1/PRF) is determined accurately, and the average velocity $v_i(t)$ during the period is obtained. By adding the product of $v_i(t)$ and ΔT to the previous object position $x_i(t)$, the next position, $x_i(t+\Delta T)$, is estimated as $x_i(t)+v_i(t)\times\Delta T$. This method has been confirmed by experiments using a water tank and has been applied to the in vivo detection of small velocity signals with sufficient reproducibility at points in the IVS of the human heart [3]. The detected velocity signal shows the rapid motion, including high frequency components with small amplitudes, which cannot be recognized by M-mode echocardiography.

Moreover, the method has been applied to multiple points preset along an ultrasonic beam in the LV wall so

that the instantaneous object positions $\{x_i(t)\}$ and the velocity signals $\{v_i(t)\}$ are obtained for these multiple points $\{i\}$ in the LV wall [1]. From the results, by deleting the parallel component, the thickness change components during myocardial contraction/relaxation are detected. Then, their spatial distribution is obtained and is superimposed on the M-mode image using a color code.

Spectrum analysis was first applied to the resultant noninvasively detected velocity signals $\{v_i(t)\}$ to identify the frequency band for the components, from 25 to 90 Hz, because of the myocardial thickening and thinning, which shows the novel possibility of diagnosis of the local myocardium [1], [3].

However, the method of measurement herein described has been developed by batch processing on an off-line system in our laboratory. The development and application of real-time processing significantly facilitate its use in clinical diagnosis and will offer a new tool for clinical examination. For example, NTG is used medically as a vasodilator for rapid treatment of angina pectoris [34]. Real-time measurement of the transient change in thickness of the heart wall or the arterial wall just after the sublingual administration of NTG will be of use in direct evaluation of the response of the heart wall or the arterial wall to the antianginal drug. At the same time, real-time monitoring during clinical intervention is essential to avoid hyper-responses, such as serious hypotension and/or arrhythmia.

Because the quantity of A/D-converted data is too great and because it is time-consuming to transfer the data from the A/D converter to a computer in the off-line system, real-time processing is indispensable to realize new clinical examination tools for evaluation of transient change of the tolerance test.

For the real-time realization of the color-Doppler method [14] and tissue Doppler imaging [35],[36], a high-speed digital circuit, such as an application-specific integrated circuit (ASIC), is employed to calculate the complex auto-correlation between the sequentially received echoes. In the tracking processing of the instantaneous position, the object position is moved along the ultrasonic beam based on the previous results from the complex autocorrelator. For more flexible processing, we employ hardware based on high-speed floating-point DSP chips and a WS.

In the hardware system employed in this study, the received echo is quadrature demodulated, and then the resultant in-phase and quadrature signals are simultaneously A/D converted at a sampling frequency of 1 MHz with a 12-bit accuracy. For these large-scale data, it is not possible to transfer them from the A/D converter to the DSP boards using the VME-bus (versa module European bus; the IEEE1024 standard) because its transfer speed is not so high. Much time-consuming processing is necessary from the A/D conversion to a real-time display of the M-mode image, the resultant waveforms, and the tracking results on the CRT (cathode-ray tube) of the WS. Thus, we employ four DSP chips. The A/D converter boards are connected directly to the DSP board. All of the processing in the four DSP should be synchronized with the transmission timing of the ultrasonic pulse, and every process assigned to each DSP chip should be terminated during the pulse repetition period, ΔT.

In this paper, after a brief description of the principle of the measurement of thickening and thinning, the architecture of the developed real-time system is described, especially with respect to the previously mentioned problems to be solved. The accuracy of the system is confirmed by experiments using a water tank, and then the real-time system is applied to in vivo experiments on the measurement of thickening and thinning in the human IVS wall and the carotid arterial wall. Finally, the system is applied to the transient evaluation of the rapid response of the change in wall thickness of the artery to the dose of NTG.

II. Principles of Measurement of Change in Thickness of the Wall

By referring to the M-mode image, which is reconstructed from the A/D-converted data, we manually preset $x_A(t_0)$ and $x_B(t_0)$ as the depth of two points, A and B, in the heart wall or arterial wall along an ultrasonic beam at a time t_0 of R-wave of the electrocardiogram (ECG) as illustrated in Fig. 1(1-b) and (2-b). We assume that both point A and point B have only a velocity component that is parallel to the direction of the beam if the direction and position of the ultrasonic beam are appropriately selected in order to be perpendicular to the wall during the cardiac cycle. The principle of the accurate detection of the change in thickness, $\Delta h_{AB}(t)$, between points A and B in the wall is briefly described as follows by referring to [3].

A. For Measurement of Instantaneous Movement $\Delta d_i(t)$ of Object (i)

RF pulses with an angular-frequency of $\omega_0 = 2\pi f_0$ are transmitted at a time interval of ΔT from an ultrasonic transducer. The ultrasonic pulse reflected by the object (i) $(i{=}A,\ B)$ is received by the same ultrasonic transducer. The output signal is amplified, and quadrature demodulation is applied to the signal. The resultant in-phase and quadrature signals for each transmitted pulse are simultaneously A/D converted at a sampling frequency $1/T_S$, and these two signals are combined into a complex signal, $y(x_i;t)$, where $x_i(t)$ and its simple expression x_i denote the depth of the object (i) from the ultrasonic transducer as shown in Fig. 2. Because $x_i(t)$ is given by the product of the acoustic velocity, c_0, and the instantaneous period, $\tau_i(t)$, required for one-way transmission from the ultrasonic transducer to the object (i), phase $\theta(x_i;t)$ of signal $y(x_i;t)$ is given by the angular frequency, ω_0, multiplied by twice the delay time, $\tau_i(t)$. Thus, the phase shift $\Delta\theta(x_i;t+\Delta T)$ of the subsequently received signals

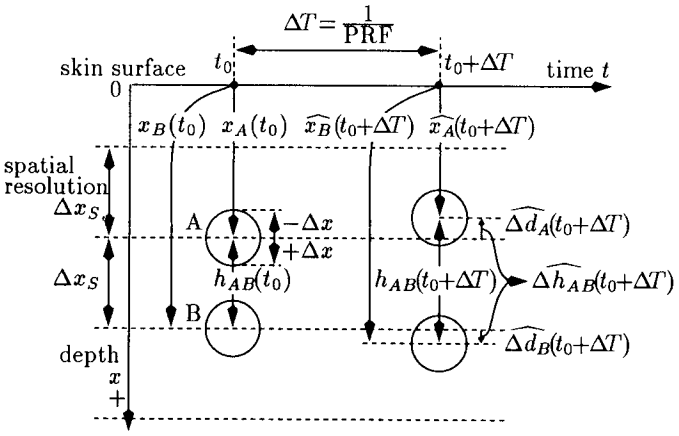

Fig. 2. An illustration of the measurement of change in thickness, $\Delta h_{AB}(t)$, between two points A and B in the pulse repetition period ΔT just after t_0.

$y(x_i; t+\Delta T)$ from $y(x_i; t)$ in the interval ΔT is given by

$$\begin{aligned}\Delta\theta(x_i; t+\Delta T) &= \theta(x_i; t+\Delta T) - \theta(x_i; t) \\ &= 2\omega_0\{\tau_i(t+\Delta T) - \tau_i(t)\} \\ &= \frac{2\omega_0}{c_0}\Delta d_i(t+\Delta T) \quad \text{[radian]}\end{aligned} \tag{1}$$

where $\Delta d_i(t+\Delta T) = x_i(t+\Delta T) - x_i(t)$ is the instantaneous movement of the object (i) in the period ΔT after time t as illustrated in Fig. 2. Then, $\Delta d_i(t+\Delta T)$ is given from the measured data by

$$\Delta d_i(t+\Delta T) = c_0 \cdot \frac{\Delta\theta(x_i; t+\Delta T)}{2\omega_0} \quad \text{(m)}. \tag{2}$$

By dividing $\widehat{\Delta d_i}(t+\Delta T)$ by ΔT, the mean velocity averaged during the ΔT is given as follows:

$$\widehat{v_i}\left(t + \frac{\Delta T}{2}\right) = \frac{\widehat{\Delta d_i}(t+\Delta T)}{\Delta T} \quad \text{(m/s)} \tag{3}$$

where $t + \Delta T/2$ shows the middle between t and $t+\Delta T$. The velocity signal and its spectrum are effective in the diagnosis of local myocardium [1].

B. For Accurate Determination of the Phase Change $\Delta\theta(x_i; t)$

Because it is essential for the measurement to determine the phase change $\Delta\theta(x_i; t)$ of (2) during period ΔT accurately, the constraint least squares method is introduced into the determination procedure of the instantaneous movement of the object position $x_i(t)$ in [3]. As described in the last paragraph of Section II C of [3], however, for the case of the sampling period $T_S = 1$ μs, which is employed in the real-time system developed in this paper, the quantized movement (lag) δ_x of the object during ΔT is less than the spatial resolution $\Delta x_S = T_S \times c_0/2 = 750\mu$m. Thus, the possible quantized lag value of δ_x is always 0, and the previously mentioned constraint least squares method exactly coincides with the well-known conventional complex auto-correlation procedure, except for the recursive adjustment of the sample window position based on the displacement estimated by the integration of the instantaneous velocity as described subsequently in (4). The range for averaging of the auto-correlation is denoted by $\pm\Delta x$.

C. For Tracking of the Object Position $x_i(t)$

The position $x_i(t)$ of the object (i) in the heart wall changes by more than 10 mm because of the heartbeat in one cardiac cycle. Even for a point in the carotid artery, the movement caused by the arrival of the pulsive wave is about several hundred micrometers. It is, therefore, necessary to track the instantaneous object position $x_i(t)$. For this purpose, by accumulating the estimate $\widehat{\Delta d_i}(t+\Delta T)$ of the instantaneous movement in (2), the next object position $\widehat{x_i}(t+\Delta T)$ is estimated by

$$\widehat{x_i}(t+\Delta T) = \widehat{x_i}(t) + \widehat{\Delta d_i}(t+\Delta T) \quad \text{(m)} \quad (i = A, B). \tag{4}$$

Thus, the instantaneous movement $\widehat{\Delta d_i}(t+\Delta T)$ and the next object position $\widehat{x_i}(t+\Delta T)$ are simultaneously determined as illustrated in Fig. 2 and are obtained as waveforms.

When the time interval, ΔT, of the transmission of the RF pulses is about 200 μs, the maximum value of the instantaneous movement, $\Delta d_i(t)$, of an object (i) in the heart wall is about 20 μm during the time interval ΔT because the velocity is less than 0.1 m/s. For the carotid artery, the maximum value of $\Delta d_i(t)$ is about 1 μm. Because the quadrature-demodulated signals are A/D converted in a sampling interval, T_S, of 1 μs in this paper, the spatial resolution $\Delta x_S = T_S \times c_0/2 = 750$ μm in the direction of depth. As illustrated in Fig. 2, therefore, the instantaneous movement, $\Delta d_i(t)$, in the heart wall and the arterial wall is much less than Δx_S and the wavelength of about 200 μm at 7 MHz or 500 μm at 3 MHz. The resultant estimate $\widehat{x_i}(t)$ of the next object position of (4) in the just mentioned procedure is represented not by a discrete value of every Δx_S but by the continuous value that is determined from the phase difference $\widehat{\Delta\theta}(x_i; t)$ in (1). Thus, accurate tracking of the object is realized by this method, and small instantaneous movement of micron order is determined.

D. For Measurement of Thickness Change in the Wall

By simultaneously applying the previously mentioned method to each of the two points A and B along the ultrasonic beam in the heart wall or the arterial wall, the instantaneous movement, $\Delta d_i(t)$, and the object positions, $x_i(t)$, are estimated for $i = A$ and B as shown in Fig. 1(1-b) or (2-b). At the beginning of this procedure, the initial positions (depth) $x_A(t_0)$ and $x_B(t_0)$ of the points at a time t_0 are manually preset. Then, at every arrival of the R-wave of the ECG, each displacement, $x_i(t)$, of each point (i) is reset to the initial position $x_i(t_0)$. For the heart

wall, $x_A(t_0)$ and $x_B(t_0)$ are in the myocardium of the IVS or in the posterior wall of the LV, and, for the carotid artery, $x_A(t_0)$ and $x_B(t_0)$ correspond to the positions on the intima and the adventitia of the anterior or posterior wall, respectively.

Let us assume that the ultrasonic beam is almost perpendicular to the wall during one cardiac cycle and that the direction of velocity of each point (i) in the wall is parallel to the direction of the ultrasonic beam. Thus, from the difference between the instantaneous object positions $x_A(t)$ and $x_B(t)$, the thickness of the local region, which is denoted by $h_{AB}(t)$, is obtained by

$$\widehat{h_{AB}}(t) = \widehat{x_B}(t) - \widehat{x_A}(t) \quad \text{(m)}. \tag{5}$$

The change in thickness, $\Delta h_{AB}(t)$, from the initial value $h_{AB}(t_0)$ at time t_0, is obtained from the estimated velocities, $v_A(t)$ and $v_B(t)$, as follows:

$$\begin{aligned}\widehat{\Delta h_{AB}}(t) &= \widehat{h_{AB}}(t) - h_{AB}(t_0) \\ &= \int_{t_0}^{t} \{\widehat{v_B}(t) - \widehat{v_A}(t)\}\mathrm{d}t \quad \text{(m)}.\end{aligned} \tag{6}$$

For the arterial wall, moreover, by dividing the absolute value of $\widehat{\Delta h_{AB}}(t)$ by the initial minimum distance $h_{AB}(t_0)$, the deformation $S_{AB}(t)$ between the points in the direction of the radius is defined by $\widehat{S_{AB}}(t) = |\widehat{\Delta h_{AB}}(t)|/h_{AB}(t_0)$. If the deformation is sufficiently small and is in the linear regime, the deformation shows strain.

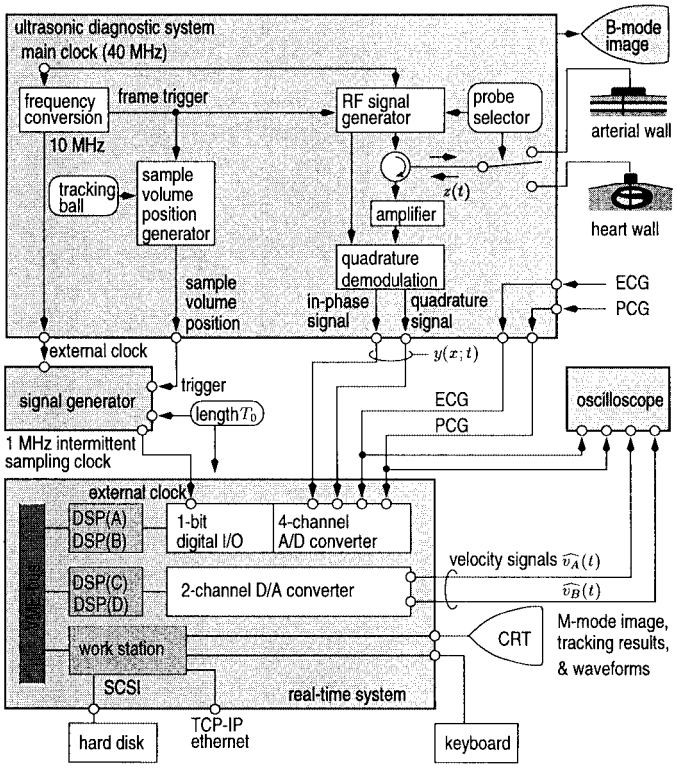

Fig. 3. An overview of the developed real-time system (lower), which is connected with the standard ultrasonic diagnostic system (upper).

III. Design of A Real-Time Measurement System

A. Architecture of the System

To realize the just mentioned procedure in real time, we have designed the following system using four high-speed floating DSP chips from DSP(A) to DSP(D) and a host WS (SUN hyperSPARC, 150 MHz, Force Computer Inc., San Jose, CA), which controls the DSP via the VME-bus. The whole structure of the real-time system is shown in Fig. 3. In the ultrasonic diagnostic equipment, the standard B-mode cross-sectional image and M-mode image are displayed to identify the measurement points on the wall. The area around a measurement point is assigned by using the sample volume, the position of which is controlled by a tracking ball. The signal $z(t)$ received by the ultrasonic transducer of Fig. 3 is amplified and quadrature demodulated in the equipment.

The resultant analytic signal $y(x;t)$ is A/D converted with a two-channel 12-bit A/D converter at a sampling interval, T_S, of 1 μs. The spatial resolution $\Delta x_S = T_S \cdot c_0/2$ in the depth direction is about 0.75 mm. As shown in Fig. 4, the analytic signal is digitized only for the period, the starting point of which is marked by the sample volume. The signal that indicates the position of the sample volume is generated in the modified ultrasonic diagnostic system and input into a signal generator (AFG2020, Tektronix,

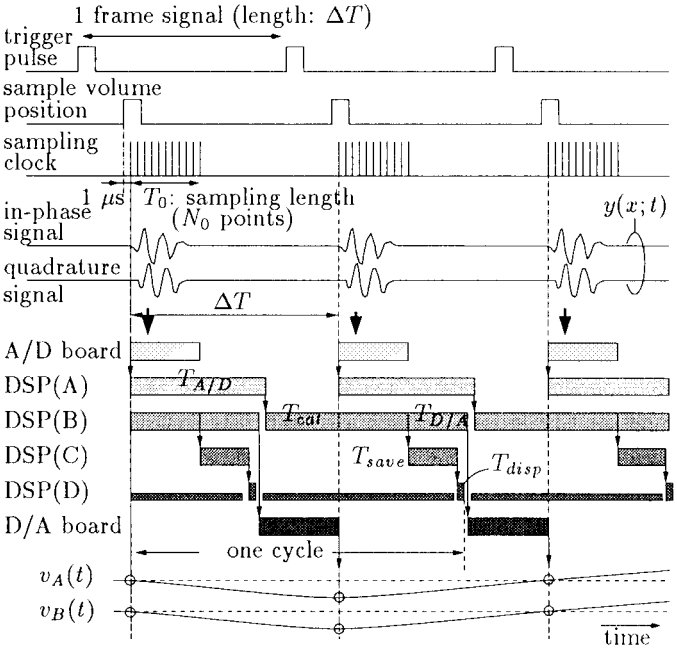

Fig. 4. Upper: An illustration explaining the timing of the sampling length and waveforms. Lower: A timing chart showing the relationships among the five tasks based on their pipelining and the parallel processing between tasks $T_{D/A}$ and T_{save}.

Wilsonville, OR) as a trigger, where the signal generator is completely synchronous with the master clock of the ultrasonic diagnostic equipment. The length, T_0, of the sampled period and the number of the data, $N_0 = T_0/T_S$, in points for each frame are assigned in advance, both in the signal generator and in the subpanel for parameter setting in the real-time system. For this intermittent digitization, a sampling clock of 1 MHz is generated only for the period T_0 by the signal generator as shown in Fig. 4. The ECG and phonocardiogram (PCG) are also digitized.

B. Tasks in the System

The following five tasks, termed $T_{A/D}$, T_{cal}, $T_{D/A}$, T_{save}, and T_{disp}, are necessary for the measurement system as shown in Fig. 4.

1. *$T_{A/D}$: Task for A/D Conversion in DSP(A):*
   - Intermittent acquisition of N_0-point in-phase and quadrature signals, ECG, and PCG using the FIFO (fast-in first-out memory) during a length of T_0 seconds from each transmitted pulse as shown in Fig. 4.
   - Conversion of the acquired signals from integer-type to floating-point-type and their packing into structure-type data $D_{A/D}$.
   - Transfer of the data $D_{A/D}$ to the DSP (B) via the communication port (CP).
2. *T_{cal}: Task for Determining Instantaneous Movement and Tracking in the DSP(B):*
   - Acquisition of data $D_{A/D}$ from task $T_{A/D}$.
   - The processing described in Section II.
     (a) calculation of complex auto-correlation in Section IIB between successively received data.
     (b) calculation of instantaneous phase shifts $\widehat{\Delta\theta}(x_A;t)$ and $\widehat{\Delta\theta}(x_B;t)$ for points A and B.
     (c) determination of the instantaneous movement, $\Delta d_A(t)$ and $\Delta d_B(t)$, of (2).
     (d) accumulation of $\Delta d_A(t)$ and $\Delta d_B(t)$ to determine the next displacement $x_A(t)$ and $x_B(t)$, which are necessary for the tracking of the object points.
   - Packing of data $\Delta d_A(t)$, $\Delta d_B(t)$, $x_A(t)$, $x_B(t)$, the original analytic signal $y(x;t)$, the ECG, and the PCG into structure-type data D_{cal}.
   - Transfer of data D_{cal} to the DSP(C) via the CP.
3. *$T_{D/A}$: Task in the DSP(B) for D/A Conversion:*
   - Conversion of the data type of $\Delta d_A(t)$ and $\Delta d_B(t)$ in the data D_{cal} from the floating-point-type to the integer-type and transfer of the resultant data to the FIFO, which is connected to the two-channel D/A converter.
4. *T_{save}: Task in the DSP(C) for Updating Data to be Saved on the Hard Disk:*
   - Transfer of data D_{cal} to update data D_{save} in a ring buffer of the global memory so that the latest 10-s data are always kept in the memory.
   - After the "SAVE" button is clicked in the main panel of the system, transfer of the current head address of data D_{save} in the ring buffer to the global memory, where the head address is necessary for the host WS to save data D_{save} on the hard disk.
   - Transfer of data D_{cal} to DSP(D).
5. *T_{disp}: Task in DSP(D) for Preparing Data to be Displayed:*
   - Down-sampling of the resultant six waveform data $\Delta d_A(t)$, $\Delta d_B(t)$, $x_A(t)$, $x_B(t)$, the ECG, and the PCG, in data D_{cal} at a sampling frequency of PRF/M_1, where M_1 is set at about 10 in the system by considering whether there is sufficient resolution.
   - Reconstruction of the M-mode image data from the absolute magnitude
     $$|y(x;t)| = \sqrt{\Re(y(x;t))^2 + \Im(y(x;t))^2}$$
     of the analytic signal $y(x;t)$. This M-mode reconstruction procedure is performed for every M_2 frame, where M_2 is set at about 50.
   - Packing of the down-sampled waveforms and the M-mode image data into a structure-type data D_{disp} and its transfer to the global memory, which is accessible from the host WS via the VME-bus.
   - Generation of the interruption to the host WS so that it will display the data.

C. Elapsed Time for Tasks

For real-time processing, each of the five tasks $T_{A/D}$, T_{cal}, $T_{D/A}$, T_{save}, and T_{disp} in the DSP should be terminated at least within the pulse repetition interval ΔT. When each data frame is N_0 points in length as shown in Fig. 4 and the complex auto-correlation in Section II B is evaluated in the range $\pm\Delta x$, the elapsed time required for each task is measured as shown in the left-hand side of Table I. In these estimates, four actual DSP chips, TMS320C40 GFL50 (refer to Appendix A for details), are employed.

When there is only one DSP chip, however, the accumulated elapsed time, T_{sngl}, required from the beginning of $T_{A/D}$ to the end of T_{disp} should be terminated within the pulse repetition interval ΔT. In this case, by the actual measurement, T_{sngl} is a function of the Δx and N_0 as follows:

$$T_{sngl} = 3.63 \times N_0 + 14.4 \times \Delta x + 129.9 \quad (\mu\text{s}). \tag{7}$$

If the PRF is 4.5 kHz or 6 kHz, T_{sngl} should be shorter than $\Delta T = 222$ μs or 167 μs, respectively. When $\Delta x = 3$ and $N_0 = 70$ points in length, which corresponds to the data length L_0 of 70 μs $\times c_0/2$=52.5 mm in the direction

TABLE I

ELAPSED TIME FOR EACH TASK. N_0 AND Δx ARE THE NUMBER OF POINTS SAMPLED IN ONE FRAME DATA AND THE EVALUATION RANGE IN THE AUTO-CORRELATION IN SECTION II B, RESPECTIVELY. THE TYPICAL ELAPSED TIME FOR EACH TASK IN THE DSP IS WHEN THE LENGTH T_0 OF EACH FRAME DATA IS 70 μS (N_0=70 POINTS) AND THE RANGE Δx IS THREE TIMES THE SPATIAL RESOLUTION Δx_S.

	Task	Elapsed time (μs)	Actual elapsed time (μs)	Arranged DSP
$T_{A/D}$:	A/D handling & data-type conversion	$1.88 \times N_0$ +16.0	147.6	DSP(A)
T_{cal}:	generation of the various waveforms	$0.64 \times N_0$+ $14.4 \times \Delta x$ +65.5	153.6	DSP(B)
$T_{D/A}$:	data-type conversion and D/A handling	$0.64 \times N_0$ +20.4	65.2	DSP(B)
T_{save}:	preparation of the data to be saved on the HD	$0.38 \times N_0$ +26.9	53.5	DSP(C)
T_{disp}:	preparation of the data to be displayed	$0.089 \times N_0$ +0.99	7.2	DSP(D)
T_{sngl}:	total time using single DSP chip	T_{cal} + $T_{D/A}$ + T_{save} + T_{disp} of (7)	427.1	By single

of depth, the elapsed time for each task is given as shown in the right-hand side of Table I, and the accumulated elapsed time, T_{sngl}, of (7) is given by

$$T_{sngl} = 427.1\mu\text{s} > \Delta T, \qquad (\Delta x = 3, N_0 = 70), \tag{8}$$

which is much longer than the pulse repetition interval, ΔT, and real-time processing cannot be realized by employing a single DSP chip.

By making free use of four DSP chips, pipelining and the parallel processing are employed to increase the throughput. The tasks T_{cal} and $T_{D/A}$ in Fig. 4 are combined and the resultant four tasks are distributed to DSP(A), DSP(B), DSP(C), and DSP(D) as shown in the extreme right of Table I and in Fig. 4. In this pipelining, each of the resultant four tasks is completed within the pulse repetition period, ΔT, which realizes the real-time processing, though these tasks cannot be realized in real time with a single DSP chip.

IV. MEASURABLE ACCURACY EVALUATED USING A WATER TANK

As in our previous paper [3], the principle of the proposed method was confirmed by an off-line system using a water tank that simulates the small vibration of the ventricle wall superimposed on the motion with a large amplitude of $\pm$7.5 mm caused by the heartbeat. Briefly, for large amplitude motion caused by the rotation (1 cycle/1 s) of the eccentric cam in the water tank [3], the tracking result of the surface of the rubber plate exactly coincided with the M-mode image. For a small vibration with a peak-to-peak amplitude of about 20 μm generated by a small vibrator (model 4810 Brüel & Kjær, Nærum, Denmark) on the eccentric cam, evaluation using the squared magnitude of the coherence function showed that a small velocity signal on a large motion was successfully detected in the frequency range from 1 Hz to 1 kHz. In this paper, the developed real-time system is applied to the same experiments.

As in the previous paper [3], the range Δx is evaluated, and 1 point is employed as its optimum valve, that is, $\Delta x = 1$ point is employed. The longitudinal velocity, c_0, in the rubber is about 1.54×10^3 m/s. The parameters of $f_0 = \omega_0/2\pi$ and the pulse repetition interval ΔT are 3 MHz and 222 μs, respectively.

Fig. 5 shows the results that are displayed in real time on the CRT of the system. Fig. 5(a) shows the M-mode image for about 3 s; this image is generated from the magnitude of the received analytic signal $y(x;t)$ in the real-time system. The tracking results $\widehat{x_A}(t)$ of point A on the surface of the rubber and $\widehat{x_B}(t)$ of point B in the rubber are superimposed on the M-mode image by the white line. The tracking results $\widehat{x_A}(t)$ and $\widehat{x_B}(t)$ of these points exactly coincide with the M-mode image.

Fig. 5(b) and (c) show the velocity signals $\widehat{v_A}(t)$ and $\widehat{v_B}(t)$, that is, the instantaneous movement, $\Delta d_A(t)$ and $\Delta d_B(t)$, of the two points, respectively. Fig. 5(e) shows the velocity signal $v_{laser}(t)$ obtained by laser Doppler velocimetry (Ono Sokki LV1300, Hakusan 1-16-1, Midori-ku, Yokohama, Japan), the output of which is connected to the PCG input terminal of the real-time system in Fig. 3. Their waveforms of $v_{laser}(t)$ and $\widehat{v_A}(t)$ are similar even in detail.

In the motion with large amplitude in the M-mode image of Fig. 5(a), however, the small components of the velocity signal $v_A(t)$ with high frequency caused by the generator cannot be recognized. One of the purposes of our method and system is to measure small velocity signals with high frequency components, which should be within the thickness of the curved line in Fig. 5(a). To evaluate quantitatively the correlation at each frequency f between the estimated signal $\widehat{v_A}(t)$ in Fig. 5(b) and $v_{laser}(t)$ in Fig. 5(e), the squared magnitude of coherence function $|\gamma_{laser \leftrightarrow us}(f)|^2$ [3, eq. (24)] between them is evaluated for the D/A output signal of $\widehat{v_A}(t)$ and $v_{laser}(t)$ using a two-channel FFT analyzer (Ono Sokki CF930). Because $|\gamma_{laser \leftrightarrow us}(f)|^2$ between these two signals is almost equal to 1 in the frequency band up to 1 kHz , there is complete correlation between these signals for each frequency component f.

On the other hand, the phase characteristics of the transfer function $H_{laser \rightarrow us}(f)$ [3, eq. (26)] from $v_{laser}(t)$

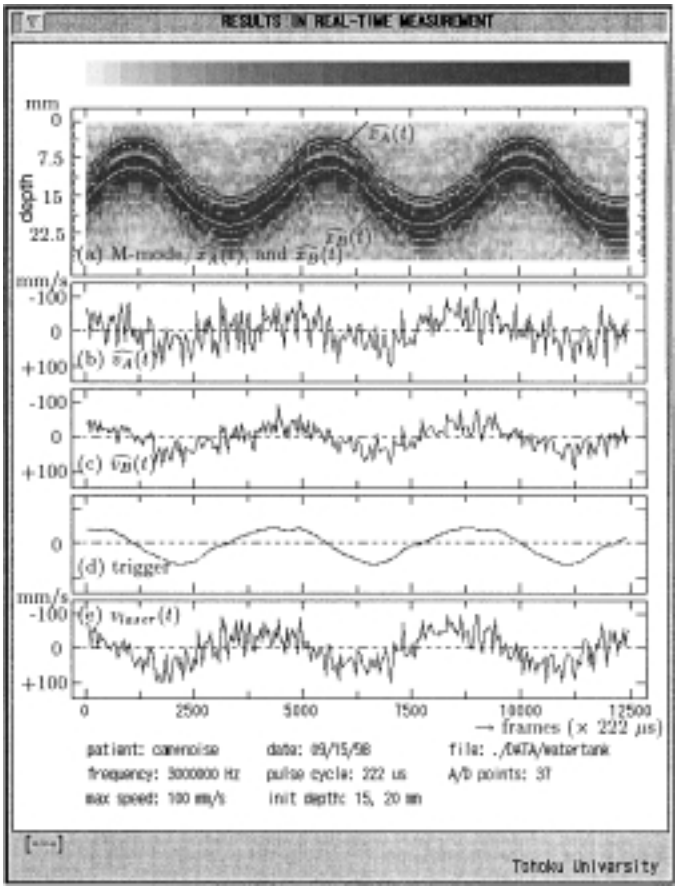

Fig. 5. The results for the experiments using the water tank [3]. (a): The estimated object motion $\widehat{x_A}(t)$ and $\widehat{x_B}(t)$ shown by white lines, superimposed on the M-mode image, (b) and (c) the estimated velocity signals $\widehat{v_A}(t)$ and $\widehat{v_B}(t)$, (d) the trigger signal generated by applying the low-pass filter to the signal in (e) (this signal is used to rearrange the object positions to $x_A(t_0)$ and $x_B(t_0)$), and (e) the velocity signal $v_{laser}(t)$ obtained by a laser Doppler velocimeter.

to $\widehat{v_{us}}(t)$ are described by an almost straight line in the frequency range up to 1 kHz. By approximating it according to the straight line $\theta = -2\pi f\tau$ [rad], and from its gradient $\frac{\partial\theta}{\partial f}$, the group delay time τ from the output of the laser Doppler velocimetry to the real-time system is about 2 ms, most of which is caused, not by the calculation, but by the delay in the A/D conversion and D/A conversion in the system. The squared magnitude of $H_{laser\to us}(f)$ is almost flat in the frequency range. From these experimental results, it is confirmed that the small vibration on the large motion can be successfully detected by this system in real time in the frequency range up to 1 kHz.

V. Measurable Lower Limit Evaluated Using A Water Tank

In addition to the previously mentioned experiments, the lower limit of the measurable velocity and the thickness change is evaluated using a rubber plate fixed in a water tank. The positions $x_A(t)$ and $x_B(t)$ of point A on the rubber surface and point B in the rubber, respectively,

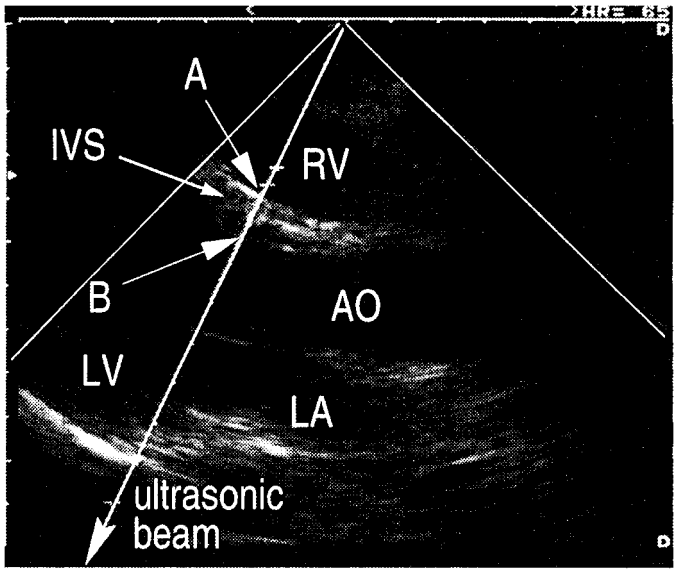

Fig. 6. A standard B-mode longitudinal-axis image showing the cross-sectional area around the detected points preset in the IVS of a presumedly healthy 39-year-old male volunteer. Points A and B are on the RV and LV of the IVS, respectively. The ultrasonic beam passing through the two points is almost perpendicular to the IVS during the measurements.

are manually preset. The distance between these points is 3 mm.

The velocity signals $\widehat{v_A}(t)$ and $\widehat{v_B}(t)$ at points A and B and the change in thickness, $\Delta h_{AB}(t)$, between them are obtained by the system; each of these three signals should be 0 if the signal-to-noise ratio is infinite. From the actual experiments, the lower limit $|v_{min}|$ of the velocity measurement is approximately given as 1 mm/s, which is less than 1/350 of the upper limit $|v_{max}| = c_0/(4f_0\Delta T) = 348$ mm/s of the measurable velocity. Because $|v_{max}|$ corresponds to the π radian of the phase-shift during the pulse repetition interval ΔT, error in the phase-shift detection is less than 0.5 degree ($= 1$[mm/s] $\times\ 180°/348$[mm/s]).

Similarly, the lower limit $|\Delta h_{min}|$ of the measurable change in thickness between these two points A and B in the system is approximately given by 1 μm, and sufficient accuracy and precision have been confirmed.

VI. In Vivo Results for IVS

First, the developed system is applied to the detection of instantaneous movement and change in thickness of the IVS of a presumedly healthy 39-year-old male volunteer. Fig. 6 shows the B-mode image, which was obtained by standard ultrasonic diagnostic equipment. Points A and B are set on the surface of the right ventricular (RV) side and the LV side of the IVS, respectively. The direction of the ultrasonic beam passing through points A and B is selected so that the beam is almost perpendicular to the IVS, as shown in Fig. 6.

Fig. 7(d) and (e) show the ECG and the PCG, respectively. The estimates of the tracking results $\widehat{x_A}(t)$ and

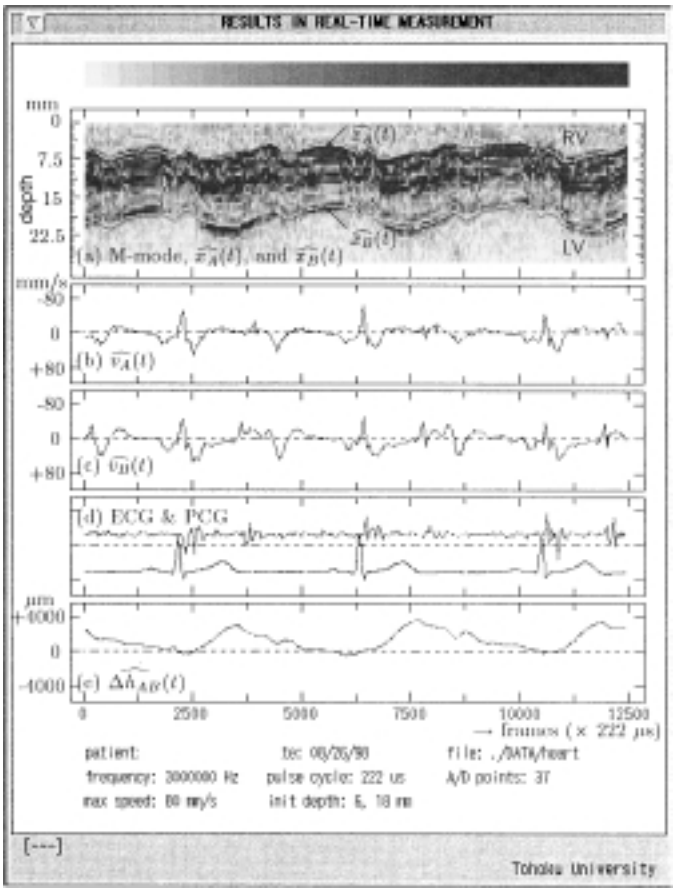

Fig. 7. In vivo experimental results for points A and B on the RV and LV of the IVS, respectively, in Fig. 6. (a) The tracking results $\widehat{x_A}(t)$ and $\widehat{x_B}(t)$ of points A and B, which are superimposed on the M-mode image; (b) and (c) the estimates of the vibration velocity signals $\widehat{v_A}(t)$ and $\widehat{v_B}(t)$ of points A and B; (d) the ECG and PCG; end (e) the change in thickness, $\widehat{\Delta h_{AB}}(t)$, of the IVS.

$\widehat{x_B}(t)$ of points A and B are superimposed on the M-mode image in Fig. 7(a). Figures 7(b) and (c) show the estimates of the velocity signals $\widehat{v_A}(t)$ and $\widehat{v_B}(t)$ of the tracked points $\widehat{x_A}(t)$ and $\widehat{x_B}(t)$, respectively. The vertical axis of Fig. 7(b) and that of Fig. 7(c) are inverted so that the negative value of the velocity, which is shown above the baseline, corresponds to the situation in which the object moves in the direction of the ultrasonic transducer on the chest wall, which is more easily understood.

The change in thickness, $\widehat{\Delta h_{AB}}(t)$, of the IVS from the thickness at the timing of the R-wave of ECG is shown in Fig. 7(e). The waveform of $\widehat{\Delta h_{AB}}(t)$ is also reproducible for a period of three heartbeats. For the systolic phase, the IVS becomes about 3 mm thicker than that of the diastolic phase, where the thickness of the IVS is about 12 mm at the end diastole.

VII. In vivo Results for the Carotid Artery

Let us apply the developed real-time system to the human carotid artery in the same volunteer as in Fig. 6 and 7. The ultrasonic frequency is 7 MHz. Fig. 8 shows a standard B-mode image. Points A and B are preset on the anterior wall and the posterior wall of the left common carotid artery, respectively. The ultrasonic beam passing through these two points is perpendicular to the wall during the measurements. Fig. 9(b) and (c) show the velocity signals $\widehat{v_A}(t)$ and $\widehat{v_B}(t)$, respectively. Their maximum velocity is about 2.5 m/s, which is about 1/20 of that for the case of the IVS in Fig. 7. The change in diameter, $\Delta\widehat{d_{AB}}(t)$, of the lumen is estimated as shown in Fig. 9(e). There is sufficient reproducibility for $\widehat{v_A}(t)$ and $\widehat{v_B}(t)$ and even for a change in diameter as small as about 250 μm.

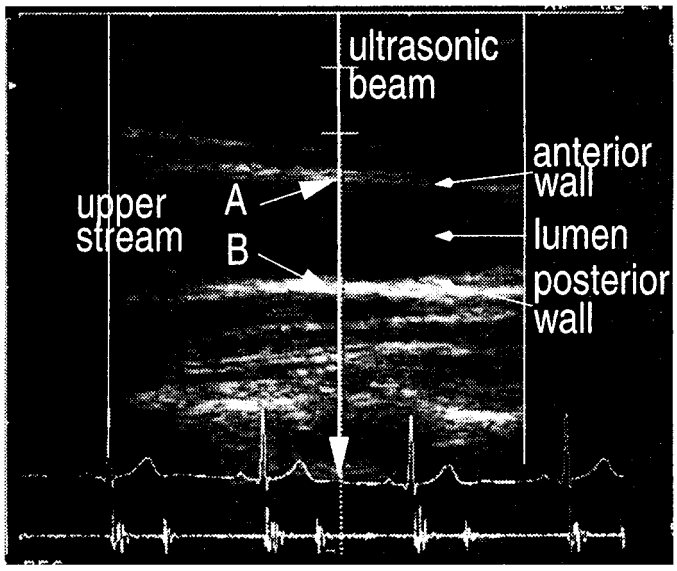

Fig. 8. A standard B-mode image showing the cross-sectional area around the detected points preset in the left common carotid artery of the same volunteer as in Fig. 6 and 7.

Next, points A and B are set on the intima and adventitia of the anterior wall of the same carotid artery, respectively. Fig. 10(b) and (c) show the velocity signals, $\widehat{v_A}(t)$ and $\widehat{v_B}(t)$, respectively. The change in thickness, $\Delta\widehat{h_{AB}}(t)$, of the anterior wall is estimated as shown in Fig. 10(e). A minute change in thickness of about 80 μm is measured with sufficient reproducibility. In the waveforms of Fig. 9(b), (c), and (e) and 10(b), (c), and (e), the dicrotic notch is obviously observed at the radiation timing of the second heart sound (II).

VIII. Transient Evaluation of Arterial Response to NTG

As described in Section I, the real-time system to measure the change in thickness of the arterial wall will offer new tools for clinical examinations. In this paper, the developed system is applied to the evaluation of a transient response of the change in thickness of the carotid artery for about the first 160 s after the sublingual administration of the spray-type NTG. The subject is a 25-year-old healthy male volunteer. The change in thickness, $\Delta h_{AB}(t)$, of the

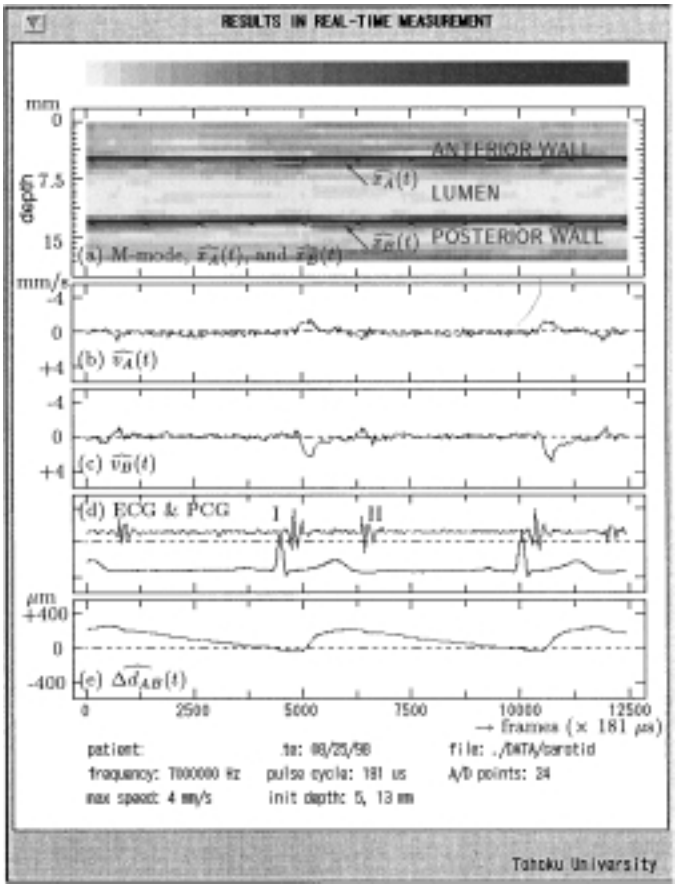

Fig. 9. In vivo experimental results of the vibration at points A and B in Fig. 8 of the left common carotid artery. (a) the tracking results $\widehat{x_A}(t)$ and $\widehat{x_B}(t)$ of points A and B, which are superimposed on the M-mode image; (b) and (c) the estimates of the vibration velocity signals $\widehat{v_A}(t)$ and $\widehat{v_B}(t)$ of points A and B; (d) the ECG and PCG; and (e) the change in diameter, $\widehat{\Delta h_{AB}}(t)$, of the lumen of the artery.

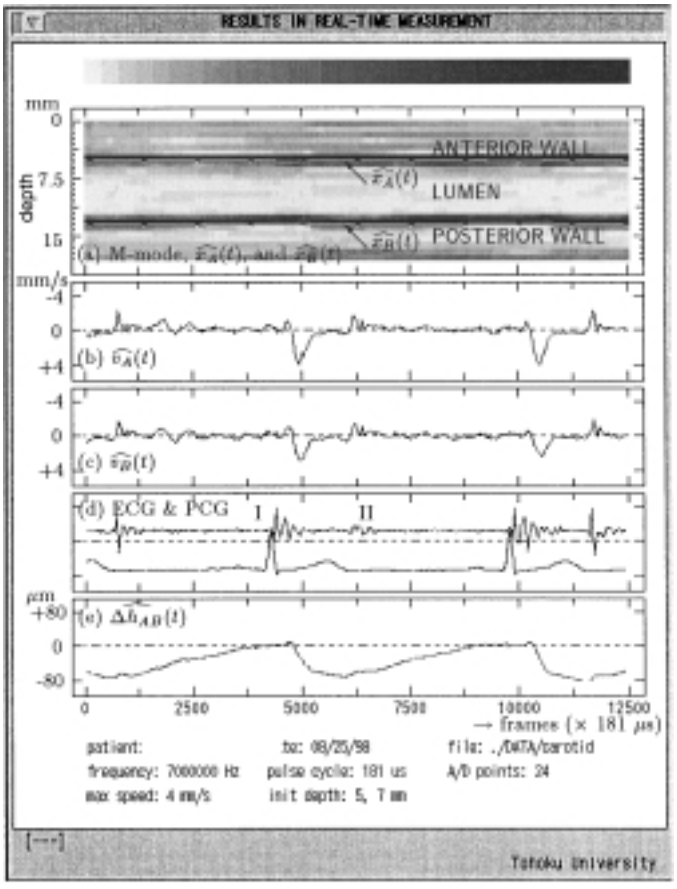

Fig. 10. In vivo experimental results of the vibration at point A on the adventitia side, and point B on the intima side of the anterior wall of the same carotid artery as in Fig. 8 and 9. (a) the tracking results $\widehat{x_A}(t)$ and $\widehat{x_B}(t)$ of points A and B, which are superimposed on the M-mode image; (b) and (c) the estimates of the vibration velocity signals $\widehat{v_A}(t)$ and $\widehat{v_B}(t)$ of points A and B; (d) the ECG and PCG; and (e) the change in thickness, $\widehat{\Delta h_{AB}}(t)$, of the anterior wall of the artery.

posterior wall of the common carotid artery and the ECG are continuously measured by the developed real-time system. The blood pressure, $p(t)$, is also continuously and noninvasively measured at the radial artery using a blood pressure manometer (Japan Colin, Jentow-7700, Komaki, Aichi, Japan).

Fig. 11 shows the transient response to the sublingual administration of NTG. For each heartbeat, the maximum of the change in thickness, $\Delta h_{AB}(t)$, is detected and is shown in Fig. 11(d). From about 20 s after the administration of NTG, the pulse rate gradually increases, the maximum blood pressure gradually decreases, and the maximum change in wall thickness increases at the same time. Thus, the arterial wall becomes compliant during this the period.

On the other hand, the maximum change in wall thickness varies widely, especially from about 20 s after the NTG administration [see the fluctuations in the trend of the change in thickness of Fig. 11(d)]. As shown in Fig. 12, however, there is a correlation between the maximum change in wall thickness of Fig. 11(d) and the pulse pressure of Fig. 11(c), which is the difference between the maximal blood pressure and the diastolic pressure. Thus, the scattering in the maximum change in wall thickness of Fig. 11(d) originates in the scattering in the pulse pressure of Fig. 11(c). From this preliminary clinical study, the response of the arterial wall to NTG is evaluated directly by the change in wall thickness for the first time. In this measurement, the real-time system is indispensable.

IX. Conclusions

In this paper we have demonstrated a novel real-time system for simultaneous measurement of velocity signals at two points preset on an ultrasonic beam by tracking the large movement of the object during the cardiac cycle. From the resultant velocity signals, the local change in thickness of the wall of the heart or the artery was also evaluated in real time. From the experiments using the water tanks and in vivo experiments, the accuracy and the performance of the system were confirmed.

The velocity signal measurement by the proposed

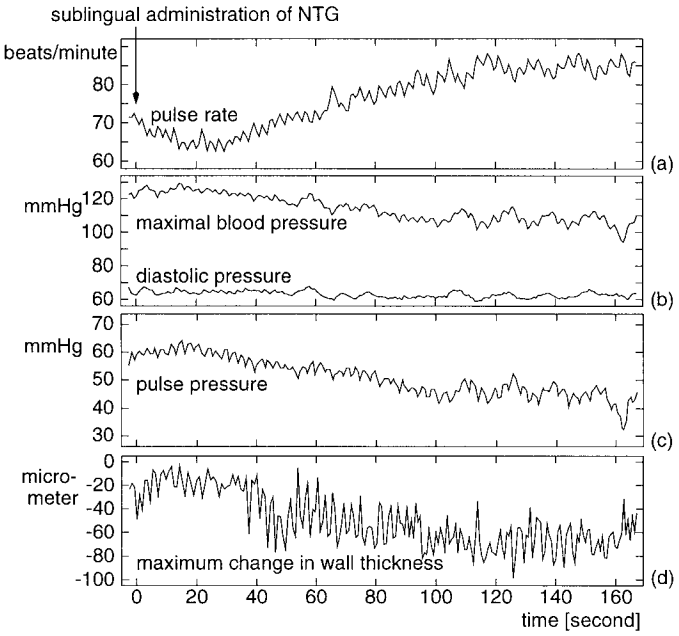

Fig. 11. The transient response of a 25-year-old healthy male subject to the administration of NTG. (a) The pulse rate detected from the interval of the R-waves in the ECG, (b) the blood pressure continuously measured at the radial artery by the manometer, (c) the pulse pressure, and (d) the maximum value of the change in thickness, $\Delta h_{AB}(t)$, of the common carotid artery detected for each heartbeat.

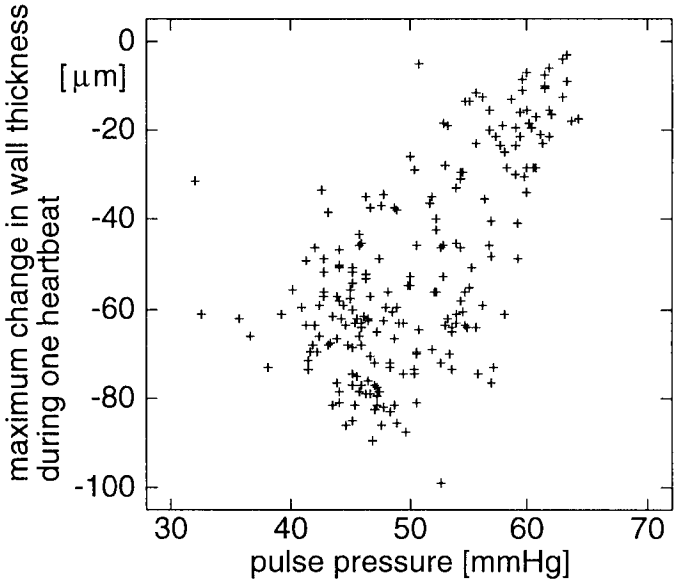

Fig. 12. The distribution of the maximum change in wall thickness in Fig. 11(d) versus the pulse pressure in Fig. 11(c).

method has the following advantages compared with conventional methods. The measurable frequency band is from dc to several hundred Hz as evaluated in Section IV; with standard ultrasonic Doppler equipment and in all of the methods reported in the literature, the measured velocity and/or the movement have been displayed only in the time domain. For them, the effective frequency band is less than 20 Hz, and the frequency components higher than 20 Hz have not been considered at all. However, the dominant component of the change in thickness is in this high frequency band [1]. Thus, for accurate detection of the change in thickness of the myocardium as shown in Fig. 7, it is essential to measure such frequency components higher than 20 Hz; our method is the first to achieve this in real time.

Because the preliminary studies in this paper were performed in healthy subjects with clear echocardiograms, much work must be done to find out how the method can be applied in a wider range of subjects and to see whether it can contribute to assessment of diseases and recovery. Further investigation of this real-time system and its clinical application to the noninvasive local diagnosis of cardiovascular disease, including that in elderly subjects, and comparison of its findings with pathological findings are being conducted.

Acknowledgments

The authors are grateful to Prof. Emeritus Noriyoshi Chubachi and Prof. Emeritus Motonao Tanaka of Tohoku University; Prof. Floyd Dunn of the Bioacoustics Research Laboratory, the University of Illinois; and Prof. Kunio Shirato, and Dr. Yasuhiko Munakata of Tohoku University School of Medicine for discussion. The authors also acknowledge the contributions of Dr. Masahiko Takano in our laboratory.

Appendix A: DSP Chips Employed

The DSP chips employed in this paper are four 32-bit floating-point digital signal processors, TMS320 C40GFL50. Each is in a 325-pin ceramic pin grid array (CPGA) package and is optimized for parallel processing by combining a high performance central processing unit (CPU) and a direct-memory-access (DMA) controller with six high speed CP that provide rapid processor-to-processor communication. The instruction cycle time is 40 ns even for floating-point multiplication. By transfer of the data via one of the six CP, effective multiprocessing and I/O-intensive application are realized. By transferring the resultant structure-type data of a task to the CP in the upper stream DSP and by accessing the data in the downstream DSP, the pipelining among the DSP is synchronized. The CPU delivers up to 30 MIPS/60 MFLOPS with a maximum I/O bandwidth of 384 Mbytes/s. The parallel run-time library is available in C language programming. Thus, the parallel processor system with pipelining allows

us to realize the measurement of instantaneous movement of the two objects preset in the heart/arterial walls and real-time evaluation of the change in thickness of these walls by tracking their instantaneous displacement accurately.

References

[1] H. Kanai, H. Hasegawa, N. Chubachi, Y. Koiwa, and M. Tanaka, "Noninvasive evaluation of local myocardial thickening and its color-coded imaging," *IEEE Trans. Ultrason., Ferroelect., Freq. Contr.*, vol. 44, no. 4, pp. 752–768, Jul. 1997.

[2] S. E. Maier, S. E. Fisher, G. C. McKinnon, O. M. Hess, H. Krayenbuehl, and P. Boesiger, "Evaluation of left ventricular segmental wall motion in hypertrophic cardiomyopathy with myocardial tagging," *Circulation*, vol. 86, pp. 1919–1928, 1992.

[3] H. Kanai, M. Sato, Y. Koiwa, and N. Chubachi, "Transcutaneous measurement and spectrum analysis of heart wall vibrations," *IEEE Trans. Ultrason., Ferroelect., Freq. Contr.*, vol. 43, no. 5, pp. 791–810, Sep. 1996.

[4] H. Hasegawa, M. Ozawa, H. Kanai, N. Chubachi, and Y. Koiwa, "Noninvasive accurate measurement of change in thickness of arterial wall and evaluation of its elastic characteristics using ultrasound," *IEEE 1997 Int. Ultrason. Symp.*, vol. 2, pp. 1169–1172, Oct. 6-8.

[5] S. Satomura, "Ultrasonic Doppler method for the inspection of cardiac function," *J. Amer. Soc. of Acoust.*, vol. 29, no. 11, pp. 1181–1185, Nov. 1957.

[6] D. W. Baker, "Pulsed ultrasonic Doppler blood-flow sensing," *IEEE Trans. Sonics Ultrason.*, vol. SU-17, no. 3, pp. 170–185, Jul. 1970.

[7] F. D. McLeod and M. Anliker, "A multiple-gate pulsed directional Doppler flowmeter," *Proc. IEEE Ultrason. Symp.*, Miami, FL, Dec. 1972, pp. 401–402.

[8] S. L. Johnson, D. W. Baker, R. A. Lute, and H. T. Dodge, "Doppler echocardiography," *Circulation*, vol. XLVIII, pp. 810–822, Oct. 1973.

[9] F. E. Barber, D. W. Baker, A. W. C. Nation, D. E. Strandness, Jr., and J. M. Reid,"Ultrasonic duplex echo-Doppler scanner," *IEEE Trans. Biomed. Eng.*, vol. BME-21, pp. 109–113, Mar. 1974.

[10] C. J. Hartley, H. G. Hanley, R. M. Lewis, and J. S. Cole,"Synchronized pulsed Doppler blood flow and ultrasonic dimension measurement in conscious dogs," *Ultrasound Med. & Biol.*, vol. 4, pp. 99–110, 1978.

[11] M. Brandestini, "Topoflow—A digital full range Doppler velocity meter," *IEEE Trans. Sonic. Ultrason.*, vol. SU-25, no. 5, pp. 287–293, Sep. 1978.

[12] E. Wildi, J. W. Knutti, H. V. Allen, and J. D. Meindl,"Dynamics and limitations of blood/muscle interface detection using Doppler power returns," *IEEE Trans. Biomed. Eng.*, vol. BME-27, no. 10, pp. 565–573, Oct. 1980.

[13] W. D. Barber, J. W. Eberhard, and S. G. Karr, "A new time domain technique for velocity measurements using Doppler ultrasound," *IEEE Trans. Biomed. Eng.*, vol. BME-32, no. 3, pp. 213–229, Mar. 1985.

[14] C. Kasai, K. Namekawa, A. Koyama, and R. Omoto,"Real-time two-dimensional blood flow imaging using an autocorrelation technique," *IEEE Trans. Sonic. Ultrason.*, vol. SU-32, no. 3, pp. 458–463, May 1985.

[15] R. M. Olson and D. K. Shelton, "A nondestructive technique to measure wall displacement in the thoracic aorta," *J. Appl. Physiol.*, vol. 32, no. 1, pp. 147–151, Jan. 1972.

[16] R. M. Olson and J. P. Cooke,"A nondestructive ultrasonic technique to measure diameter and blood flow in arteries," *IEEE Trans. Biomed. Eng.*, vol. BME-21, pp. 168–171, 1974.

[17] J. O. Arndt, "The diameter of the intact carotid artery in man and its change with pulse pressure," *Pflüegers Archiv.*, vol. 301, pp. 230–240, 1968.

[18] D. J. Mozersky, D. S. Sumner, D. E. Hokanson, and D. E. Strandness, Jr.,"Transcutaneous measurement of the elastic properties of the human femoral artery," *Circulation*, vol. XLVI, pp. 948–955, Nov. 1972.

[19] A.P.G. Hoeks, C. J. Ruissen, P. Hick, and R. S. Reneman,"Transcutaneous detection of relative changes in artery diameter," *Ultrasound Med. & Biol.*, vol. 11, no. 1, pp. 51–59, 1985.

[20] W. T. Kemmerer, R. W. Ware, H. F. Stegall, J. L. Morgan, and R. Kirby, "Blood pressure measurement by Doppler ultrasonic detection of arterial wall motion," *Surgery, Gynecology and Obstetrics*, vol. 131, pp. 1141–1147, Dec. 1970.

[21] K. Lindström, K. Marsal, G. Gennser, L. Bengtsson, M. Benthin, and P. Dahl, "Device for measurement of fetal breathing movements, 1. The TD-recorder. A new system for recording the distance between two echogenerating structures as a function of time," *Ultrasound Med. & Biol.*, vol. 3, pp. 143–151, 1977.

[22] D. E. Hokanson, D. E. Strandness, Jr., and C. W. Miller, "An echo-tracking system for recording arterial wall motion," *IEEE Trans. Sonic Ultrason.*, vol. SU-17, no. 3, pp. 130-132, Jul. 1970.

[23] D. E. Hokanson, D. J. Monzersky, S. D. Sumner, and D. E. Strandness, Jr., "A phase-locked echo tracking system for recording arterial diameter changes in vivo," *J. Appl. Physiol.*, vol. 32, no. 5, pp. 728–733, May 1972.

[24] D. N. White and R. J. Stevenson, "Transient variations in the systolic pulsations in amplitude of intracranial echoes, their artificial origin," *Neurology*, vol. 26, pp. 683–689, 1976.

[25] C. F. Olsen, "Doppler ultrasound: a technique for obtaining arterial wall motion parameters," *IEEE Trans. Sonic Ultrason.*, vol. SU-24, no. 6, pp. 354–358, Jun. 1977.

[26] L. W. Korba, R.S.C. Cobbold, and A. J. Cousin, "An ultrasonic imaging and differential measurement system for the study of fetal respiratory movements," *Ultrasound Med. & Biol.*, vol. 5, pp. 139–149, 1979.

[27] I. Rapoport and A. J. Cousin,"New phase-lock tracking instrument for foetal breathing monitoring," *Med. & Biol. Eng. & Comp.*, vol. 20, pp. 1–6, Jan. 1982.

[28] D. H. Groves, T. Powalowski, and D. N. White, "A digital technique for tracking moving interfaces," *Ultrasound Med. & Biol.*, vol. 8, no. 2, pp. 185–190, 1982.

[29] C. J. Hartley, H. Litowitz, R. S. Rabinovitz, W. X. Zhu, J. E. Chelley, L. H. Michael, and R. Bolli,"An ultrasonic method for measuring tissue displacement: technical details and validation for measuring myocardial thickening," *IEEE Trans. Biomed. Eng.*, vol. BME-38, no. 8, pp. 735–747, Aug. 1991.

[30] L. S. Wilson and D. E. Robinson, "Ultrasonic measurement of small displacements and deformations of tissue," *Ultrasonic Imaging*, vol. 4, pp. 71–82, 1982.

[31] C. J. Hartley, L. A. Latson, L. H. Michael, C. L. Seidel, R. M. Lewis, and M. L. Entman, "Doppler measurement of myocardial thickening with single epicardial transducer," *Amer. J. Physiol.*, vol. 245, pp. H1066–1072, 1983.

[32] A.P.G. Hoeks, P. J. Brands, F.A.M. Smeets, and R. S. Reneman,"Assessment of the Distensibility of Superficial Arteries," *Ultrasound Med. & Biol.*, vol. 16, no. 2, pp. 121–128, 1990.

[33] R. W. Stadler, W. C. Karl, and R. S. Lees, "The application of echo-tracking methods to endothelium-dependent vasoreactivity and arterial compliance measurements," *Ultrasound Med. & Biol.*, vol. 22, no. 1, pp. 35–42, 1996.

[34] *Churchill's Illustrated Medical Dictionary.*, New York, NY: Churchill Livingstone Inc., 1989.

[35] K. Miyatake, N. Tanaka, M. Yamagishi, N. Yamazaki, Y. Mine, and M. Hirama, "Clinical application of newly developed color-coded tissue Doppler echocardiography in detection of abnormal ventricular wall motion," *J. Amer. Soc. Echocardiography*, vol. 6, no. 3, part 2, p. S19, May–Jun. 1993.

[36] N. Yamazaki, Y. Mine, A. Sano, M. Hirama, and K. Miyatake, "Analysis of ventricular wall motion using color-coded tissue Doppler imaging system," *Jpn. J. Appl. Phys.*, vol. 33, no. 5B, pp. 3141–3146, 1994.

Hiroshi Kanai (A'88–M'91)was born in Matsumoto, Japan, on November 29, 1958. He received a B.E. degree from Tohoku University, Sendai, Japan, in 1981 and the M.E. and the Ph. D. degrees, also from Tohoku University, in 1983 and in 1986, both in electrical engineering.

From 1986 to 1988, he was with the Education Center for Information Processing, Tohoku University, as a research associate. From 1990 to 1992, he was a lecturer in the Department of Electrical Engineering, Faculty of Engineering, Tohoku University. Since 1992, he has been an associate professor in the Department of Electrical Engineering, Faculty of Engineering, Tohoku University. His present interest is in ultrasonic measurement and digital signal processing for diagnosis of heart diseases and arteriosclerosis.

Dr. Kanai is a member of the Acoustical Society of Japan, the Institute of Electronics Information and Communication Engineering of Japan, the Japan Society of Mechanical Engineers, the Japan Society of Ultrasonics in Medicine, Japan Society of Medical Electronics and Biological Engineering, the Institute of Electrical Engineers of Japan, the Japanese Circulation Society, and the Japanese College of Cardiology.

Yoshiro Koiwa was born in Sendai, Japan, in 1944. He graduated from Tohoku University, Sendai, Japan, in 1969. He received his M.D. degree from Tohoku University in 1977.

He is presently Associate Professor of the First Department of Internal Medicine of Tohoku University. His main research interest is cardiovascular disease, especially cardiac function and heart failure.

Dr. Koiwa is a member of American Federation for Clinical Research, the Japanese Circulation Society, the Japan Society of Ultrasonics in Medicine, and the Japan Society of Medical Electronics and Biological Engineering.

Jianping Zhang was born in Shanghai, China on July 7, 1962. He received his B.S. degree from Shanghai University of Science and Technology (currently Shanghai University), Shanghai, China, in 1984, and M.A. degreee from Commerce Graduate School of Commerce, Waseda University, Tokyo, Japan, in 1992.

From 1992 to 1998, he was with System Design Service Corporation as a software engineer. He has been engaged in developing digital signal processing systems in various fields, such as active noise control, robust adaptive beam forming, and telecommunications. Almost every system he has developed is a real-time system, and he is experienced in the analysis and design of time-critical systems using state-of-the-art multiple DSP tasking.